Available online at www.sciencedirect.com
SCIENCE DIRECT®
PERGAMON
International Journal of Heat and Mass Transfer 46 (2003) 2087–2093
International Journal of HEAT and MASS TRANSFER
www.elsevier.com/locate/ijhmt

3D numerical modeling of non-isotropic turbulent buoyant helicoidal flow and heat transfer in a curved open channel

Yong-Ming Shen [a,*], Chiu-On Ng [b], Hao-Qing Ni [a]

[a] State Key Laboratory of Coastal and Offshore Engineering, Dalian University of Technology, Dalian 116023, PR China
[b] Department of Mechanical Engineering, The University of Hong Kong, Pokfulam Road, Hong Kong, PR China

Received 29 September 2002

Abstract

A 3D non-isotropic algebraic stress/flux turbulence model is employed to simulate turbulent buoyant helicoidal flow and heat transfer in a rectangular curved open channel. The prediction shows that, unlike the isothermal flow, there are two major and one minor secondary flow eddies in a cross section of thermally stratified turbulent buoyant helicoidal flow in a curved open channel. The results compare favorably with available experimental data. The thermocline in a curved channel is thicker than that in a straight channel. All of these is the result of complex interaction between the buoyant force, the centrifugal force and the Reynolds stresses. The turbulent flow in a curved channel is obviously non-isotropic: the turbulence fluctuations in vertical and radial directions are lower in magnitude than that in the axial direction, which illustrates the suppression of turbulence due to buoyant and centrifugal forces. The results are of significant practical value to engineering works such as the choice of sites for intake and pollutant-discharge structures in a curved river.

Keywords: Curved open channel; Non-isotropic turbulent flow; Stratification; Buoyancy; 3D numerical modeling

1. Introduction

The disposal of waste heat into natural watercourses from industrial and power generation processes poses an increasing threat to the world's fresh water resources. It is important, on the part of environmental hydraulic engineers, to understand the hydrodynamics of the flow and heat transport in curved channels in order to be able to assess the impact caused by thermal pollution on a natural stream. Turbulent buoyant helicoidal flow in a curved channel can be considered as one of the most complex fluid-flow situations encountered in the environment owing to the fact that the flow is turbulent and strongly three dimensional. There are marked secondary motions in cross sections normal to the streamwise direction. Induced by complex interactions between the buoyant force, the centrifugal force and the Reynolds stresses, the secondary motions can be organized to emerge in the form of three-dimensional helicoidal flow that may in return modify the characteristics of the primary flow, sediment transport and heat transfer in the channel. In particular, these secondary motions can significantly enhance the rate of lateral spreading of substances released to the channel. Knowledge of the hydrodynamic and heat transport processes in curved open-channel flow is of significant practical value, for such knowledge is required for the design of preventive measures against silting and for the choice of sites for intake and pollutant-discharge structures in a river. Despite the practical importance, the understanding of the hydrodynamics of turbulent buoyant helicoidal flow and heat transfer has been very limited.

In the past two decades, various 3D numerical models have been used to simulate curved channel flow, which include notably the works by Leschziner and Rodi [1], De Vriend [2], Galmes and Lakshminarayana [3], Demuren and Rodi [4], Shimizu et al. [5], Demuren [6], Sinha et al. [7], Ye and McCorquodale [8], Wu et al.

* Corresponding author. Fax: +86-411-470-8526.
E-mail address: ymshen@dlut.edu.cn (Y.-M. Shen).

0017-9310/03/$ - see front matter
doi:10.1016/S0017-9310(02)00501-X

Nomenclature

B	channel width
c's	empirical constants in turbulence model
g	gravitational acceleration
h	thickness
H	water depth
k	turbulent kinetic energy
K_a	von Karman's constant in log-law (about 0.4)
L	length
P	mean pressure
Q	discharge
r	radial coordinate
r_c	radius of curvature of curved channel center
r_i	radius of curvature of inner bank (convex bank)
r_o	radius of curvature of outer bank (concave bank)
t	time
T	mean temperature
T^*	dimensionless mean temperature
V_0	characteristic velocity (bulk velocity through the inlet)
v_r, v_φ, v_z	fluctuating velocity components in r, φ and z directions, respectively
V_r, V_φ, V_z	mean velocity components in r, φ and z directions, respectively
V_r^*, V_φ^*, V_z^*	dimensionless mean velocity components in r, φ and z directions, respectively
z	vertical coordinate

Greek symbols

β	volumetric expansion coefficient
ε	turbulent kinetic energy dissipation rate
θ	fluctuating temperature
ρ	fluid density
φ	angular polar coordinate

Superscript

bar	time-averaged quantity

Subscripts

1	upper warmer-water at the entrance of the straight inlet reach
2	lower cooler-water at the entrance of the straight inlet reach
c	curved channel center
i	inner bank (convex bank)
in	straight inlet reach
o	outer bank (concave bank)
out	straight outlet reach
r	radial direction
s	water surface
z	vertical direction
φ	tangential direction

[9], and many others. Until recently, the 3D numerical modeling of curved channel flow has mostly been confined to isothermal non-buoyant flow simulations. It is well known that for isothermal flow in a curved channel the major secondary flow is caused by the centrifugal force. In addition, a minor secondary eddy is induced by the normal stress gradient, which can only be realistically accounted for with a 3D non-isotropic turbulent flow model [10–12]. On the other hand, there does not seem to exist any numerical studies on the non-isothermal turbulent buoyant helicoidal flow in a curved channel. Only some limited experimental investigations have been performed on this kind of flow [13]. Owing to the added effects due to buoyancy, the secondary motions for non-isothermal turbulent flows can differ in pattern dramatically from those for isothermal flows. The non-isothermal turbulence structure is generally highly non-isotropic and non-homogeneous. The commonly used turbulence models that are based on an isotropic eddy viscosity assumption will be deficient when applied to turbulent buoyant helicoidal flows [14–16].

In this paper, an efficient modified non-isotropic algebraic stress/flux turbulence model with the proper consideration of stress convection is presented. The model can allow for more physics to be taken into account than the conventional k–ε models in terms of pressure-strain interaction (redistribution of stresses) and turbulence/body force (buoyancy, centrifugal force, etc.) interactions. The model is used to simulate non-isotropic turbulent buoyant helicoidal flow in a 180° open channel bend. The results are compared with some available data that have been published previously [13].

2. Mathematical model

It is important to recognize that turbulent motion is essentially stochastic and chaotic [17]. In order to predict the gross or average behavior of turbulent buoyant helicoidal flow, a mathematical model must be established. The basic foundation for modeling of turbulent flow is Navier–Stokes equations. Based on the instan-

taneous equations for conservation of mass, momentum and thermal energy, a statistical approach is taken here. We start out by defining a turbulent quantity to be the sum of the mean value of the quantity and its fluctuating part. Taking ensemble average of the instantaneous equations, we get the time-averaged governing equations for 3D non-isotropic turbulent buoyant helicoidal flows and heat transfer. The modified algebraic stress/flux turbulence model is employed for the closure of modeling the Reynolds stresses and fluxes in the time-averaged governing equations. On simplifying the Reynolds stress transport equations into algebraic expressions, the non-gradient convection terms is retained in the present model since they may be comparable to the gradient convection terms [18]. Thus, the governing equations for non-isotropic turbulent buoyant helicoidal flows and heat transfer may be written in terms of cylindrical polar coordinates (r, φ, z) as follows:

Continuity equation:

$$\frac{\partial \rho}{\partial t}+\frac{1}{r}\frac{\partial}{\partial r}(r\rho V_r)+\frac{1}{r}\frac{\partial}{\partial \varphi}(\rho V_\varphi)+\frac{\partial}{\partial z}(\rho V_z)=0 \tag{1}$$

Radial momentum equation:

$$\begin{aligned}&\frac{\partial}{\partial t}(\rho V_r)+\frac{1}{r}\frac{\partial}{\partial r}(r\rho V_r V_r)+\frac{1}{r}\frac{\partial}{\partial \varphi}(\rho V_\varphi V_r)+\frac{\partial}{\partial z}(\rho V_z V_r)\\&\quad=-\frac{\partial P}{\partial r}+\rho\frac{V_\varphi^2}{r}+\rho\frac{\overline{v_\varphi v_\varphi}}{r}-\frac{1}{r}\frac{\partial}{\partial r}(r\rho\overline{v_r v_r})\\&\qquad-\frac{1}{r}\frac{\partial}{\partial \varphi}(\rho\overline{v_r v_\varphi})-\frac{\partial}{\partial z}(\rho\overline{v_r v_z})\end{aligned} \tag{2}$$

Streamwise (or tangential) momentum equation:

$$\begin{aligned}&\frac{\partial}{\partial t}(\rho V_\varphi)+\frac{1}{r}\frac{\partial}{\partial r}(r\rho V_r V_\varphi)+\frac{1}{r}\frac{\partial}{\partial \varphi}(\rho V_\varphi V_\varphi)+\frac{\partial}{\partial z}(\rho V_z V_\varphi)\\&\quad=-\frac{1}{r}\frac{\partial P}{\partial \varphi}-\rho\frac{V_r V_\varphi}{r}-\rho\frac{\overline{v_r v_\varphi}}{r}-\frac{1}{r}\frac{\partial}{\partial r}(r\rho\overline{v_\varphi v_r})\\&\qquad-\frac{1}{r}\frac{\partial}{\partial \varphi}(\rho\overline{v_\varphi v_\varphi})-\frac{\partial}{\partial z}(\rho\overline{v_\varphi v_z})\end{aligned} \tag{3}$$

Vertical momentum equation:

$$\begin{aligned}&\frac{\partial}{\partial t}(\rho V_z)+\frac{1}{r}\frac{\partial}{\partial r}(r\rho V_r V_z)+\frac{1}{r}\frac{\partial}{\partial \varphi}(\rho V_\varphi V_z)+\frac{\partial}{\partial z}(\rho V_z V_z)\\&\quad=-\frac{\partial P}{\partial z}-\frac{1}{r}\frac{\partial}{\partial r}(r\rho\overline{v_z v_r})-\frac{1}{r}\frac{\partial}{\partial \varphi}(\rho\overline{v_z v_\varphi})\\&\qquad-\frac{\partial}{\partial z}(\rho\overline{v_z v_z})+\rho g\beta T\end{aligned} \tag{4}$$

Energy equation:

$$\begin{aligned}&\frac{\partial}{\partial t}(\rho T)+\frac{1}{r}\frac{\partial}{\partial r}(r\rho V_r T)+\frac{1}{r}\frac{\partial}{\partial \varphi}(\rho V_\varphi T)+\frac{\partial}{\partial z}(\rho V_z T)\\&\quad=-\frac{1}{r}\frac{\partial}{\partial r}(r\rho\overline{v_r\theta})-\frac{1}{r}\frac{\partial}{\partial \varphi}(\rho\overline{v_\varphi\theta})-\frac{\partial}{\partial z}(\rho\overline{v_z\theta})\end{aligned} \tag{5}$$

Turbulent kinetic energy equation:

$$\begin{aligned}&\frac{\partial}{\partial t}(\rho k)+\frac{1}{r}\frac{\partial}{\partial r}(r\rho V_r k)+\frac{1}{r}\frac{\partial}{\partial \varphi}(\rho V_\varphi k)+\frac{\partial}{\partial z}(\rho V_z k)\\&\quad=\frac{1}{r}\frac{\partial}{\partial r}\left(rc_k\rho\frac{k^2}{\varepsilon}\frac{\partial k}{\partial r}\right)+\frac{\partial}{\partial z}\left(\rho c_k\frac{k^2}{\varepsilon}\frac{\partial k}{\partial z}\right)+G_k\\&\qquad+\rho g\beta\overline{v_z\theta}-\rho\varepsilon\end{aligned} \tag{6}$$

Turbulent kinetic energy dissipation rate equation:

$$\begin{aligned}&\frac{\partial}{\partial t}(\rho\varepsilon)+\frac{1}{r}\frac{\partial}{\partial r}(r\rho V_r\varepsilon)+\frac{1}{r}\frac{\partial}{\partial \varphi}(\rho V_\varphi\varepsilon)+\frac{\partial}{\partial z}(\rho V_z\varepsilon)\\&\quad=\frac{1}{r}\frac{\partial}{\partial r}(rc_\varepsilon\rho\frac{k^2}{\varepsilon}\frac{\partial\varepsilon}{\partial r})+\frac{\partial}{\partial z}(\rho c_\varepsilon\frac{k^2}{\varepsilon}\frac{\partial\varepsilon}{\partial z})+c_{\varepsilon1}\frac{\varepsilon}{k}G_k\\&\qquad+c_{\varepsilon3}\frac{\varepsilon}{k}\rho g\beta\overline{v_z\theta}-\rho c_{\varepsilon2}\frac{\varepsilon^2}{k}\end{aligned} \tag{7}$$

State equation:

$$\begin{aligned}\rho=&(0.102027692\times10^{-2}+0.677737262\times10^{-7}\times T\\&-0.905345843\times10^{-8}\times T^2\\&+0.864372185\times10^{-10}\times T^3-0.642266188\\&\times10^{-12}\times T^4+0.105164434\times10^{-17}\times T^7\\&-0.104868827\times10^{-19}\times T^8)\times9.8\times10^5\end{aligned} \tag{8}$$

and stress and heat flux algebraic expressions, such as

$$\begin{aligned}\overline{v_z v_r}=&\frac{kr}{\rho(kV_r+c_1\varepsilon r)}\left\{(1-c_2)\left[-\rho\left(\overline{v_r v_r}\frac{\partial V_z}{\partial r}\right.\right.\right.\\&+\overline{v_r v_\varphi}\frac{\partial V_z}{r\partial\varphi}+\overline{v_r v_z}\frac{\partial V_z}{\partial z}+\overline{v_z v_r}\frac{\partial V_r}{\partial r}+\overline{v_z v_\varphi}\frac{\partial V_r}{r\partial\varphi}\\&\left.\left.\left.+\overline{v_z v_z}\frac{\partial V_r}{\partial z}\right)+\frac{\rho}{r}\overline{v_\varphi v_z}V_\varphi+\frac{1}{(1-c_2)}\frac{1}{r}\rho V_\varphi\overline{v_\varphi v_z}\right]\right.\\&\left.+(1-c_3)\rho g\beta\overline{v_r\theta}\right\}\end{aligned} \tag{9}$$

$$\begin{aligned}\overline{v_z\theta}=&-\frac{kr}{(kV_r+c_{T1}\varepsilon r)}\left[\overline{v_z v_r}\frac{\partial T}{\partial r}+\overline{v_z v_\varphi}\frac{\partial T}{r\partial\varphi}+\overline{v_z v_z}\frac{\partial T}{\partial z}\right.\\&+(1-c_{T2})\left(\overline{v_r\theta}\frac{\partial V_z}{\partial r}+\overline{v_\varphi\theta}\frac{\partial V_z}{r\partial\varphi}+\overline{v_z\theta}\frac{\partial V_z}{\partial z}\right)\\&\left.-(1-c_{T3})\beta g\overline{\theta\theta}\right]\end{aligned} \tag{10}$$

$$\overline{\theta\theta}=-2\frac{kr}{(kV_r+2c_{\theta1}\varepsilon r)}\left(\overline{v_r\theta}+\overline{v_\varphi\theta}\frac{1}{r}\frac{\partial T}{\partial\varphi}+\overline{v_z\theta}\frac{\partial T}{\partial z}\right) \tag{11}$$

where

$$\begin{aligned}G_k=&-\rho\left[\overline{v_r v_\varphi}\left(\frac{\partial V_\varphi}{\partial r}+\frac{1}{r}\frac{\partial V_r}{\partial\varphi}-\frac{V_\varphi}{r}\right)+\overline{v_\varphi v_\varphi}\left(\frac{1}{r}\frac{\partial V_\varphi}{\partial\varphi}+\frac{V_r}{r}\right)\right.\\&+\overline{v_z v_\varphi}\left(\frac{1}{r}\frac{\partial V_z}{\partial\varphi}+\frac{\partial V_\varphi}{\partial z}\right)+\overline{v_r v_r}\frac{\partial V_r}{\partial r}\\&\left.+\overline{v_z v_r}\left(\frac{\partial V_z}{\partial r}+\frac{\partial V_r}{\partial z}\right)+\overline{v_z v_z}\frac{\partial V_z}{\partial z}\right]\end{aligned} \tag{12}$$

Similar expressions can be given for $\overline{v_r v_r}$, $\overline{v_\varphi v_\varphi}$, $\overline{v_z v_z}$, $\overline{v_r v_\varphi}$, $\overline{v_\varphi v_z}$, $\overline{v_\varphi \theta}$ and $\overline{v_r \theta}$. In the equations presented above, the symbols have the following meanings: an overbar denotes time averaging; subscripts r, φ and z are the radial, tangential and vertical directions, respectively; t time; V_r, V_φ and V_z are mean velocity components in r, φ and z directions, respectively; v_r, v_φ and v_z are fluctuating velocity components in r, φ and z directions, respectively; P is mean pressure; ρ is fluid density; g is gravitational acceleration; β is volumetric expansion coefficient; T is mean temperature; θ is fluctuating temperature; k is turbulent kinetic energy; ε is turbulent kinetic energy dissipation rate; c_1, c_2, c_3, c_k, c_ε, $c_{\varepsilon 1}$, $c_{\varepsilon 2}$, $c_{\varepsilon 3}$, c_{T1}, c_{T2}, c_{T3} and $c_{\theta 1}$ are all empirical constants whose values have been given in the literature [10,17].

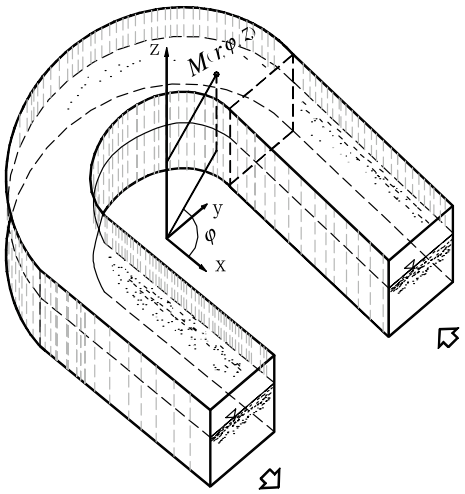

Fig. 1. Flow configuration and coordinate system.

3. Numerical computation and physical discussions

3.1. The problem

The mathematical model described above is applied to turbulent buoyant helicoidal flow in a 180° open channel bend as shown in Fig. 1, for which the experimental data presented in He et al. [13] can be used for comparison. This flow configuration is a suitable test case for the present model because it can reveal many of the basic features such as stratification and secondary motions resulting from the interactions between the buoyant force, the centrifugal force and the Reynolds stresses. The geometry consists of a U-shaped smooth channel of rectangular cross section with 0.4 m in width and 0.6 m in height. The channel is made up of a 180° bend with two straight inlet and outlet reaches of the same cross section before and after the bend. The geometrical parameters of the computed domain are: the channel width $B = 0.40$ m; the total water depth $H = 0.29$ m; the radius of curvature of the centerline of the bend $r_c = 1.3$ m; the radius of curvature of the inner bank (convex bank) $r_i = 1.1$ m; the radius of curvature of the outer bank (concave bank) $r_o = 1.5$ m; the length of the inlet reach $L_{in} = 4.0$ m; the length of the outlet reach $L_{out} = 3.4$ m.

A thermally stratified flow is created by joining two streams of water, which are initially separated by a splitter plate, and have different velocities and temperatures before mixing. The streams are discharged from the upper and lower inlets into the channel. The upper water is warmer than the lower one so that the denser stream is below the lighter one and the thermal stratification is stable. At the entrance the total water depth is 0.29 m, in which the upper depth is 0.02 m and the lower depth is 0.27 m. Throughout the experiments, some special measures were taken in order to keep all the parameters constant. The experimental data obtained by He et al. [13] is adopted here in order to test the accuracy of the model. The experimental conditions are listed in Table 1. The meanings of the parameters in Table 1 are: h_1 and h_2 are the thicknesses of the upper warmer-water and the lower cooler-water at the entrance of the straight inlet reach, respectively; Q_1 and Q_2 are the discharges of the upper warmer-water and the lower cooler-water at the entrance of the straight inlet reach, respectively; T_1 and T_2 are the temperatures of the upper warmer-water and the lower cooler-water at the entrance of the straight inlet reach, respectively; ρ_1 and ρ_2 are the densities of the upper warmer-water and the lower cooler-water at the entrance of the straight inlet reach, respectively.

3.2. Boundary conditions

As shown in Fig. 1, there are four types of boundaries to be considered for the solution domain, namely inlet, outlet, walls and the free surface. Boundary conditions are in general required for all dependent variables at all boundaries of the solution domain. In the

Table 1
Experimental conditions

The parameters for upper warmer-water				The parameters for lower cooler-water			
h_1 (m)	Q_1 (cm^3/s)	T_1 (°C)	ρ_1 (kg/m^3)	h_2 (m)	Q_2 (cm^3/s)	T_2 (°C)	ρ_2 (kg/m^3)
0.02	750	32	995.05	0.27	4890	22	997.80

present case, however, boundary conditions for V_r, V_φ, V_z, k and ε are not required at the outflow plane because the related equations are partially parabolic. At the boundary of inlet, the velocity is calculated by the empirical formula under a certain discharge. Turbulence variables are determined according to the distribution of velocity. Temperature and density are given according to the experimental data. The free surface is treated as a slip plane (rigid-lid approximation) and the symmetry condition is adopted. Because of the bounds imposed by the free surface, the turbulent kinetic energy dissipation rate ε_s is determined by the empirical relation: $\varepsilon_s = C_\mu^{3/4} k_s^{3/2}/(0.07 K_a H)$, where $K_a = 0.4$ is von Karman's constant; k_s is the turbulent kinetic energy at the free surface; H is water depth. On the channel wall, the no-slip boundary condition is used. The heat and mass transfer through the walls is negligible, in which case a zero normal gradient is the proper wall boundary condition. For the grid nodes immediately adjacent to the wall boundary, the viscous sublayer is treated by the wall function approximation. At the boundary of outlet, boundary conditions are only required for the pressure since the related equations are partially parabolic.

3.3. Results and discussions

In the present work, a finite control volume procedure [19] is adopted. In this procedure, a non-uniform grid is set up in the computational region. Denser grids are employed in the region where the variation of flow variables is more rapid. The discrete governing equations are obtained by integrating the original differential equations over the control volume. This integration is equivalent to considering a balance for the individual variables over the control volume. Because the equations are non-linear and coupled with each other, the solution is obtained by using the SIMPLE algorithm with iteration and under-relaxation. The numerical model described above is employed to simulate 3D non-isotropic turbulent buoyant helicoidal flows and heat transfer in a 180° open channel bend.

Figs. 2–7 show the computed results and the corresponding experimental results at the cross section 90° in the channel. To facilitate comparison, the following dimensionless variables are introduced:

$$V_r^* = V_r/V_0, \quad V_z^* = V_z/V_0, \quad V_\varphi^* = V_\varphi/V_0,$$
$$T^* = (T - T_2)/(T_1 - T_2)$$

where V_0 is the characteristic velocity (bulk velocity through the inlet), V_r^*, V_φ^* and V_z^* are the dimensionless components of mean velocity in r, φ and z directions respectively, T^* is the dimensionless mean temperature.

It can be seen from Figs. 2–5 that the primary streamwise flow is accompanied with strong secondary motions. There are two secondary eddies of comparable

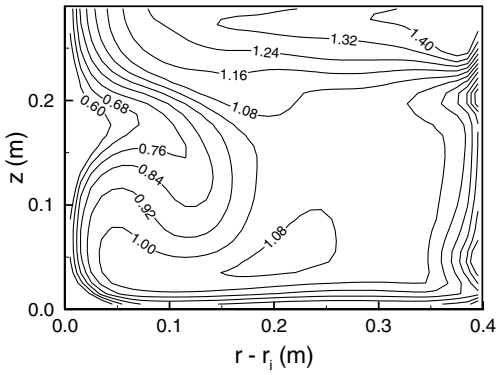

Fig. 2. Calculated streamwise velocity contours at cross section 90° in 180° open channel bend.

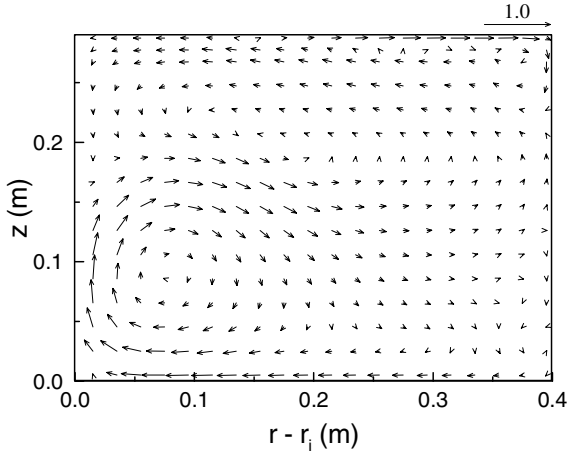

Fig. 3. Calculated secondary flow velocity vectors at cross section 90° in 180° open channel bend.

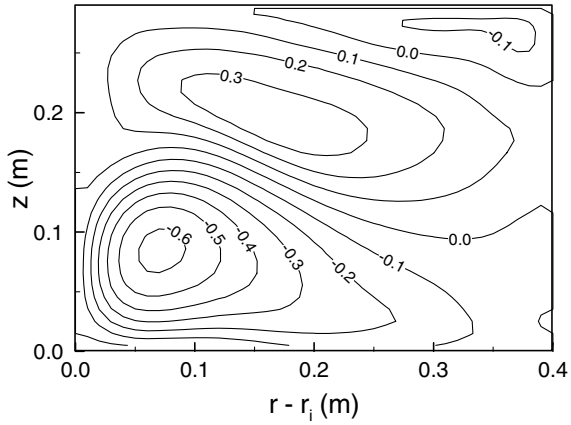

Fig. 4. Calculated secondary flow streamlines at cross section 90° in 180° open channel bend.

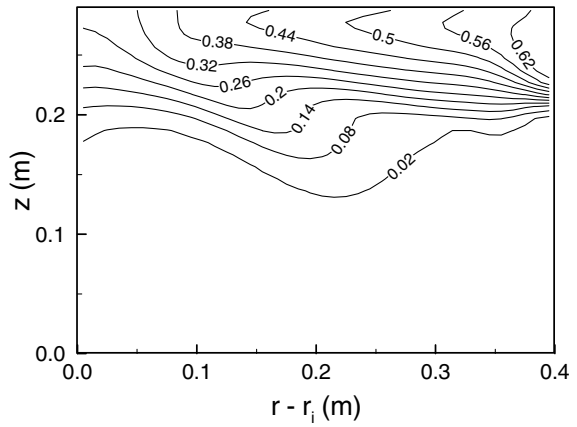

Fig. 5. Calculated temperature contours at cross section 90° in 180° open channel bend.

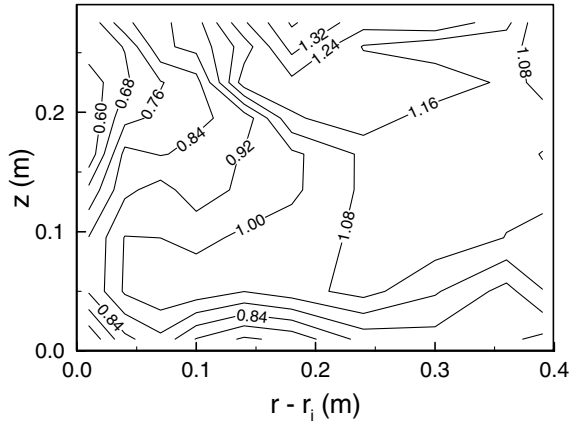

Fig. 6. Measured streamwise velocity contours at cross section 90° in 180° open channel bend.

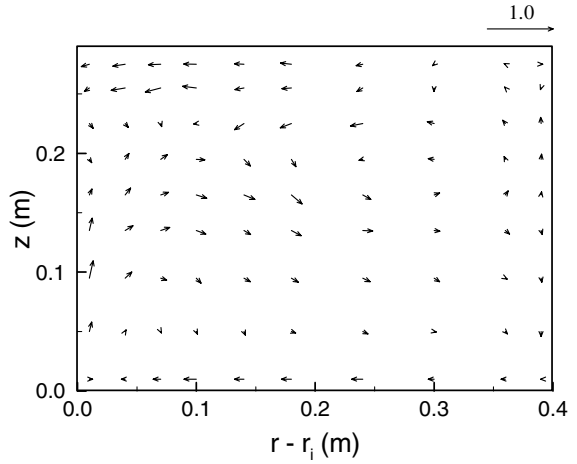

Fig. 7. Measured secondary flow velocity vectors at cross section 90° in 180° open channel bend.

size, which rotate in opposite directions. This is in sharp contrast to isothermal flow in which the secondary motions consist of only one major eddy and a minor eddy, rotating in opposite directions. The buoyancy effect causes a thermocline that acts as a barrier separating the cooler-water below from mixing with the warmer water above. At the same time, the eddy on the interface stirs up a second eddy in the upper warmer-water region. The boundary between these two eddies is situated right in the thermocline. It can be observed from Fig. 2 that the maximum velocities are located near the concave bank in the warmer-water region and the minimum ones near the convex bank in cooler-water region. The streamwise velocity contours near the bottom and the concave bank are crowded and almost parallel to the wall. The warmer layer is thicker near the concave bank than near the convex bank owing to a higher tangential velocity or larger centrifugal force in the warmer-water layer. On the other hand, the convection and mixing due to secondary flows makes the thermocline thicker in a curved channel than that in a straight channel. Obviously, the turbulence is non-isotropic not only near the wall and free surface, but also in the thermocline. In these regions, the vertical and radial turbulence intensity is smaller than tangential turbulence intensity. This is the effect of turbulence suppression due to buoyancy and centrifugal forces, which is in good agreement with the experiments [13]. Comparison of Figs. 2–4 with Figs. 6 and 7 show that the present results can reflect the actual flow pattern with good accuracy. There is some quantitative discrepancy between the calculations and experiments, which can be ascribed to the inaccuracy of laser Doppler measurements in low-velocity regions. The turbulence model of course also needs further improvement on, for examples, the stress/flux modeling, and the numerical diffusion.

4. Conclusions

(a) A modified algebraic stress/flux turbulence model has been applied to the problem of non-isotropic turbulent buoyant helicoidal flow and heat transfer in a curved open channel that is preceded and followed by straight reaches. The calculated results are found in good agreement with available experimental data. The model takes into account the non-isotropic stresses due to buoyant forces and centrifugal forces or interaction between the buoyant force, the centrifugal force and the Reynolds stresses.

(b) The numerical results reveal that two comparable eddies rotating in opposite directions are formed in cross sections of the turbulent buoyant helicoidal flow in a curved open channel. The boundary

between the two eddies is located right in the thermocline. The flow is obviously different from the case for isothermal flow, which has only one major eddy due to the centrifugal effect and a minor one due to the normal stress gradient.

(c) The secondary flow leads to a thicker thermocline of the flow in a curved channel than that in a straight channel and a deeper warmer-water layer near the concave bank than near the convex bank.

(d) The turbulence in buoyant flow in a curved channel is markedly non-isotropic: the turbulence intensity is smaller in the vertical and radial directions than the tangential direction due to turbulence suppression by buoyancy and centrifugal forces. The flow and heat transfer in a curved channel are dramatically different from those in a straight channel. These results are of significant practical value to the design of engineering works, such as in choosing locations for intake and pollutant-discharge structures in a natural river.

Acknowledgements

This research is sponsored by the Hong Kong Research Grants Council (RGC) under grant no. HKU 7081/02E, the National Science Fund for Distinguished Young Scholars under grant no. 50125924, the Research Fund for the Doctoral Program of Higher Education under grant no. 2000014112, and Natural Science Fund of Liaoning Province under grant no. 2001101073.

References

[1] M.A. Leschziner, W. Rodi, Calculation of strongly curved open channel flow, ASCE J. Hydraul. Div. 105 (10) (1979) 1297–1314.

[2] H.J. De Vriend, Velocity redistribution in curved rectangle channels, J. Fluid Mech. 107 (6) (1981) 423–439.

[3] J.M. Galmes, B. Lakshminarayana, Turbulence modeling for three-dimensional shear flows over curved rotating bodies, AIAA J. 22 (10) (1984) 1420–1428.

[4] A.O. Demuren, W. Rodi, Calculation of flow and pollutant dispersion in meandering channels, J. Fluid Mech. 172 (11) (1986) 63–92.

[5] Y. Shimizu, H. Yamaguchi, T. Itakura, Three-dimensional computation of flow and bed deformation, ASCE J. Hydraul. Eng. 116 (9) (1990) 1090–1108.

[6] A.O. Demuren, A numerical model for flow in meandering channels with natural bed topography, Water Resour. Res. 29 (4) (1993) 1269–1277.

[7] S.K. Sinha, F. Sotiropoulos, A.J. Odgaard, Three-dimensional numerical model for flow through natural rivers, ASCE J. Hydraul. Eng. 124 (1) (1998) 13–24.

[8] J. Ye, J.A. McCorquodale, Simulation of curved open channel flows by 3D hydrodynamic model, ASCE J. Hydraul. Eng. 124 (7) (1998) 687–698.

[9] W. Wu, W. Rodi, T. Wenka, 3D numerical modeling of flow and sediment transport in open channels, ASCE J. Hydraul. Eng. 126 (1) (2000) 4–15.

[10] W. Rodi, Turbulence Models and Their Application in Hydraulics, third ed., in: IAHR Monograph, Balkema, Rotterdam, The Netherlands, 1993.

[11] H. Iacovides, B.E. Launder, Turbulent momentum and heat-transport in square sectioned ducts rotating in orthogonal mode, Numer. Heat Trans. 12 (4) (1987) 475–491.

[12] M.D. Su, R. Friedrich, Numerical simulation of fully-developed flow in a curved duct of rectangular cross-section, Int. J. Heat Mass Trans. 37 (8) (1994) 1257–1268.

[13] Y.Y. He, Y.F. Fu, F.T. Li, J.Y. Jiang, D.C. Fu, Preliminary experimental investigation on the properties of the thermal density flow in open channel bend, in: Proceedings of the Second National Symposium on Environmental Hydraulics, Beijing, China, 1992, pp. 199–205.

[14] D. Cokljat, B.A. Younis, Second-order closure study of open channel flows, ASCE J. Hydraul. Eng. 121 (2) (1995) 94–105.

[15] Y.M. Shen, Y.C. Li, A.T. Chwang, Quasi-three-dimensional refined modelling of turbulent flow and water quality in coastal waters, Sci. China, Series E 39 (4) (1996) 342–353.

[16] Y.M. Shen, W.Q. Zhao, H.Q. Ni, The two-fluid model of turbulent buoyant recirculating two-phase flow, Sci. China, Series A 36 (9) (1993) 1129–1139.

[17] C.J. Chen, S.Y. Jaw, Fundamentals of Turbulence Modeling, Taylor & Francis, Washington, DC, 1998.

[18] J. Zhang, S. Nieh, L.X. Zhou, A new version of algebraic stress model for simulating strongly swirling turbulent flows, Numer. Heat Trans., Part B 22 (1) (1992) 49–62.

[19] S.V. Patankar, Numerical Heat Transfer and Fluid Flow, McGraw-Hill, New York, 1980.